Optimal Off-Line Trajectory Planning of Hybrid Fuel Cell/Gas Turbine Power Plants

Shivakumar Kameswaran and L. T. Biegler
Dept. of Chemical Engineering, Carnegie Mellon Univ., Pittsburgh, PA 15213

S. Tobias Junker and Hossein Ghezel-Ayagh
FuelCell Energy, Inc., Danbury, CT 06813

DOI 10.1002/aic.11089
Published online January 4, 2007 in Wiley InterScience (www.interscience.wiley.com).

A nonlinear programming (NLP) framework is developed to determine optimal operating policies for hybrid fuel cell/gas turbine power systems. The approach consists of a dynamic model of the power plant, reformulated as an index one differential algebraic equation (DAE) system. A dynamic optimization framework is developed where the constraints include the dynamic model of the plant. The system model is then discretized using Radau collocation on finite elements and formulated in the AMPL modeling environment. This allows for the straightforward solution of dynamic optimization problems using large-scale NLP solvers. IPOPT is the NLP solver used in this study. Program links were provided to Matlab/Simulink to visualize and interpret the results. The formulation of a dynamic optimization problem was focused on determination of optimal operating trajectories for tracking power plant load variations. Efficiency measures were also included as a part of the dynamic optimization problem to maximize efficiency while tracking the desired load profile. Results from 18 case studies show that the dynamic optimization can be performed quickly with excellent results. The applicability of the dynamic optimization framework for the estimation of feed fuel concentrations is also demonstrated. © 2007 American Institute of Chemical Engineers *AIChE J,* 53: 460–474, 2007

Keywords: fuel cells, power generation, dynamic optimization, nonlinear programming, model-based control, state estimation

Introduction

Fuel Cell/Gas Turbine (FC/GT) systems embody an approach to using fossil fuels efficiently, cleanly, and affordably for production of electricity.[1] The FC/GT power plants are expected to have negligible emissions while achieving projected efficiencies of 75% based on the fuel's lower heating value (LHV) for natural gas.[2] As an alternative to natural gas, these systems can also be configured to operate on fuels such as coal gas or biomass derivatives (such as from wood gasification or waste-water treatment plants).[3]

Correspondence concerning this article should be addressed to L. T. Biegler at biegler@cmu.edu

FC/GT hybrid systems have a high degree of coupling between fuel cell, gas turbine, and heat recovery units. The overall dynamics are nonlinear with varying degrees of interdependencies among the processes. The design of an FC/GT hybrid power plant has to address the operational constraints and details of the component performance characteristics.[4]

Dynamic simulation has proven to be a powerful design tool for the study of the transient behavior of FC/GT hybrid systems.[5] Additionally, dynamic modeling provides a platform for investigating advanced control algorithms and dynamic optimization routines during the design phase. The utility of dynamic simulation of fuel cell systems in the design of various fuel cell power plants has been explored elsewhere.[6]

The dynamic operation and control of FC/GT hybrid power plants requires a synergy of operation among subsystems, increased reliability of operation, and reduction in maintenance and downtime. The control strategy plays a significant role in system stability and performance as well as ensuring the protection of equipment for maximum plant life.[7,8] In particular, optimal profiles are required for load changes, dynamic scheduling of setpoints, and feedforward control moves for the system controllers, as well as estimation of disturbances and data reconciliation.

The primary objective of this article is the development, implementation/solution, and documentation of a dynamic optimization framework for FC/GT hybrid power plants. To enable dynamic optimization of these systems, a simultaneous problem formulation was implemented and coupled to a large-scale nonlinear programming (NLP) algorithm. Using this framework, various operating scenarios, such as increasing and decreasing load changes at different rates, were optimized. The dynamic optimization framework is also modified to maximize plant efficiency while tracking the desired load profile. Furthermore, this formulation was demonstrated for the estimation of variations in fuel composition.

Process Description

FC/GT systems are combined cycles composed of integration of a high temperature (>873 K) fuel cell, either a Molten Carbonate Fuel Cell (MCFC) or Solid Oxide Fuel Cell (SOFC), and a gas turbine. The FC/GT cycle based on a variant of MCFC technology with internal reforming capability (under the trade names Direct FuelCell®/Turbine and DFC/T®) has taken a lead in responding to recent demands for increased fuel-to-electric power conversion efficiency. Recently, factory tests of an Alpha DFC/T hybrid power plant, fabricated by integration of a 250kW Direct FuelCell® (DFC®) stack with a 60kW Capstone MicroTurbine™, was successfully concluded with a near record setting performance.[9] The Alpha DFC/T hybrid power plant achieved a power generation level of greater than 320 kW at 56% (LHV) while operating on natural gas. Figure 1 shows a simplified process flow diagram.

The key feature of this process is a high level of integration between the fuel cell subsystem and the turbine subsystem. The turbine provides process air to the fuel cell, while the fuel cell provides heat to the turbine. Both subsystems produce electric power. Power from the turbine is produced in a high-speed generator; DC power from the fuel cell is inverted to AC prior to being sent to the utility grid.

In the fuel cell subsystem, feed water humidifies natural gas in a humidifier/heat exchanger (HH) prior to entering the fuel cell anode. In the anode methane is reformed into hydrogen and carbon dioxide, and its chemical potential is converted to electrical energy. The anode exhaust, which contains some unreacted fuel, is mixed with hot air and oxidized completely in the anode gas oxidizer (AGO). An oxidizer bypass (dotted line) facilitates temperature control of the oxidizer. Hot effluent from the oxidizer heats the turbine inlet, enters the fuel cell cathode, preheats the compressor outlet, and finally provides heat to the humidifier.[10,11]

In the turbine subsystem, ambient air is first compressed and then preheated in a low temperature recuperator (LTR) using fuel cell waste heat. The compressed hot air is heated further using a high temperature recuperator (HTR) located between the oxidizer and the fuel cell cathode. An HTR bypass (dotted line) facilitates temperature control of the cathode inlet temperature. Hot air leaving the HTR is expanded through the turbine section before being sent to the AGO. The turbine drives both the compressor and a permanent magnet generator. During system startup additional heat is provided by an electric heater (EHTR), and the generator works as a motor as long as the turbine cannot provide sufficient torque to operate the compressor.

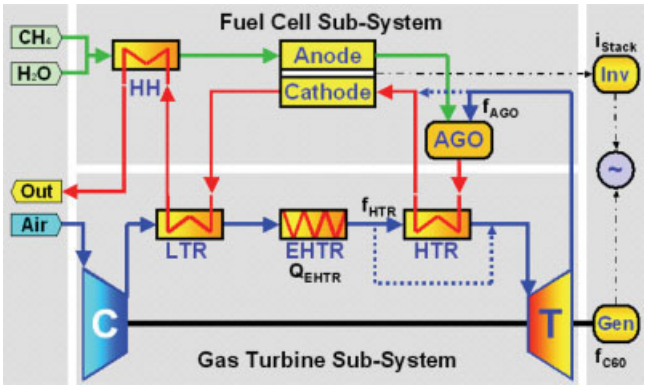

Figure 1. Flow diagram of FuelCell Energy's Direct FuelCell/Turbine® (DFC/T®) hybrid system.

[Color figure can be viewed in the online issue, which is available at www.interscience. wiley.com.]

Overview

The article is organized as follows. The next section gives an overview of the modeling approach, the dynamic simulation, and the conventional control strategy. An introduction to the dynamic optimization problem is presented in the third section, along with details of the mathematical reformulation of the model, which is a prerequisite for dynamic optimization. Subsequent to a detailed discussion of the framework for optimal operating policies, several case studies are presented in the fourth section. In the fifth section, we present an extension of the dynamic optimization framework for online composition estimation along with some case studies. We conclude the article in the last section along with directions for future work.

Dynamic Process Model

Direct FuelCell

The principle of the internally reformed carbonate fuel cell is shown in Figure 2. The carbonate fuel cell uses alkali metal carbonate mixtures as the electrolyte to transfer ions between the fuel cell electrodes. The basic electrochemistry, as illustrated in Figure 2, involves formation of carbonate ($CO_3^{=}$) at the cathode by the combination of oxygen, carbon dioxide, and two electrons; transport of the carbonate ions to the anode through the carbonate electrolyte; and finally, reaction of carbonate ions with hydrogen at the anode, producing water, carbon dioxide, and two electrons. Carbon monoxide can also be utilized as a fuel.

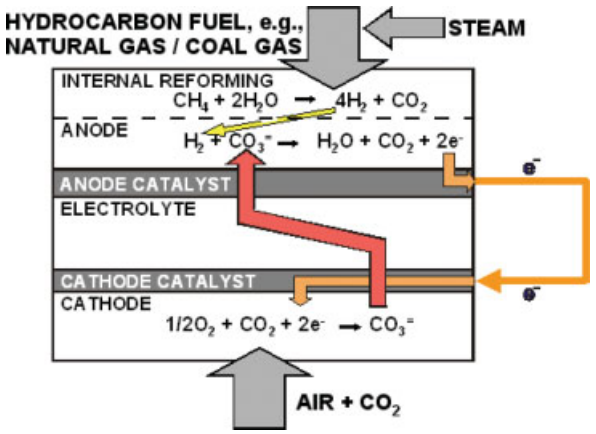

Figure 2. Internally reformed carbonate fuel cell principle of operation.

[Color figure can be viewed in the online issue, which is available at www.interscience.wiley.com.]

The fuel cell is described by a lumped parameter model, where the anode and cathode are modeled as well mixed volumes with interchange of mass (ions) through the electrolyte matrix separating the two sides. Seven chemical components are considered in this study and identified by the set NC = $\{H_2, CH_4, CO, CO_2, H_2O, N_2, O_2\}$. This leads to 7 differential mole balance equations in both the anode and cathode ($k=\{a,c\}$), given by:

$$\frac{dx_{k,i}}{dt} = \frac{\dot{N}_k^{\text{in}}(x_{k,i}^{\text{in}} - x_{k,i}) - x_{k,i}\sum_{j=1}^{7} R_{k,j} + R_{k,i}}{N_k} \equiv \frac{f_{k,i}}{N_k}, \quad \forall i \in NC, \text{k} \in \{a,c\} \quad (1)$$

where $\dot{N}_k^{\text{in}}$ and $x_{k,i}^{\text{in}}$ are the inlet molar flowrate and composition into the anode/cathode compartment, respectively, N_k and $x_{k,i}$ are the total moles and the composition in the anode/cathode compartment, and $R_{k,i}$ represents the rate of production of species $i \in NC$ in the anode/cathode due to chemical and electrochemical reactions. The functions $f_{k,i}$ are defined to simplify the notation in this work.

Three reactions take place in the anode: (1) steam reformation, (2) water-gas shift, and (3) the electrochemical half reaction. In the cathode, only the electrochemical half reaction takes place.

In the first reaction, methane is reformed with steam to carbon monoxide and hydrogen:

$$CH_4 + H_2O \rightarrow CO + 3H_2$$

The methane reforming reaction is assumed to be at equilibrium. The equilibrium expression is given by:

$$K_1 = \frac{\exp(E_3 - E_4/T)}{\exp(E_1 - E_2/T)} = p_a^2 \frac{x_{CO}(x_{H_2})^3}{x_{CH_4}x_{H_2O}} \quad (2a)$$

In the second reaction, carbon monoxide reacts with water to form carbon dioxide and hydrogen:

$$CO + H_2O \rightarrow CO_2 + H_2$$

This reaction is very fast and is also assumed to be at equilibrium:

$$K_2 = \exp(E_1 - E_2/T) = \frac{x_{CO_2}x_{H_2}}{x_{CO}x_{H_2O}} \quad (2b)$$

These two reactions are lumped together with the anode reactions. Because these reactions are at equilibrium, the reaction rates r_1 (reforming) and r_2 (water-gas shift) are not known directly, and are determined in the third section as part of the reformulation of the differential algebraic equation (DAE) system. Finally, electrochemical reactions occur at the anode and cathode. For the MCFC the cell reactions are:

$$\text{Cathode}: 1/2\ O_2 + CO_2 + 2e^- \rightarrow CO_3^{2-}$$

$$\text{Anode}: H_2 + CO_3^{2-} \rightarrow H_2O + CO_2 + 2e$$

The rates for the above electrochemical reactions are given by Faraday's law of electrolysis:

$$r_3 = \frac{i_{\text{stack}}A_{\text{cell}}n_{\text{cell}}}{2F}$$

where i_{stack} is the stack current density, A_{cell} is the active cell area, n_{cell} is the number of cells in the stack, and $F = 96485$ C/mol is the Faraday constant.

In summary, the reaction rate vectors whose elements appear in Eq. 1 for the anode and cathode are given by:

$$\text{Anode}: R_a = [3r_1 + r_2 - r_3, -r_1, r_1 - r_2, r_2 + r_3, -r_1 - r_2 + r_3, 0, 0]^T$$

$$\text{Cathode}: R_c = [0, 0, 0, -r_3, 0, 0, -0.5r_3]^T$$

Assuming that energy accumulates only in the stack solid mass, gas mixtures are ideal, and exit stream temperatures are equal to the solid stack temperature, the energy conservation equation is:

$$\frac{dT_{\text{stack}}}{dt} = \frac{\sum_{k=a,c}\left[\dot{N}_k^{\text{in}}\sum_{i=1}^{7}((x_{k,i}\bar{h}_{k,i})^{\text{in}} - (x_{\text{k,i}}\bar{h}_{k,i})) - \sum \text{R}_{k,i}\sum(x_{k,i}\bar{h}_{k,i})\right] - P_{\text{dc}} - Q_{\text{loss}}}{(mc_p)_s + \frac{1}{T_{\text{stack}}}\sum_{k=a,c}\left[\dot{N}_k^{\text{in}}\sum_{i=1}^{7}(x_{k,i}\bar{h}_{k,i})\right]} \equiv f_T \quad (3)$$

where m is the total stack mass, $c_p(T)$ is the average stack heat capacity, $\bar{h}_{k,j}$ is the molar enthalpy of component i in anode/cathode, P_{dc} is the stack DC power, and Q_{loss} is the heat loss. Molar enthalpies are computed as a function of temperature from the heat capacities, and P_{dc} is given by the product of stack current, cell voltage, and number of cells.

Constitutive equations for the average cell voltage are based on the Nernst equation as well as empirical relationships for activation, concentration, and ohmic polarizations of the form:

$$V_{\mathrm{cell}} = f(i_{\mathrm{stack}}, T_{\mathrm{stack}}, p_a, p_c) \tag{4a}$$

$$P_{\mathrm{dc}} = n_{\mathrm{cell}} V_{\mathrm{cell}} i_{\mathrm{stack}} A_{\mathrm{cell}} \tag{4b}$$

where p_a and p_c are the respective anode and cathode pressures.[12] A complete set of stack model equations and transient validation against a sub-scale test stack is provided in ref. 13.

Balance-of-plant and micro-turbine

In addition to the micro-turbine, balance-of-plant (BOP) components in the DFC/T hybrid system include the humidifier, heat exchangers, and the anode gas oxidizer (AGO). Heat exchangers are modeled via a steady-state energy balance using the ε-NTU method[14] and the heat transfer coefficients derived from the process specifications in the Alpha DFC/T power plant. The humidifier model is assumed to be a steady-state unit operation comprising a water evaporator, a mixer for mixing steam and natural gas, and a heat exchanger for heating the humidified natural gas. Because the AGO operates with a high air-to-fuel ratio, complete oxidation of the CH_4, CO, and H_2 exhaust from the anode is assumed. The differential equations for mass and energy are simplified versions of Eqs. 1 and 3, respectively. A detailed description for these types of component models can be found in ref. 15.

The modified Capstone C60 MicroTurbine$^{\mathrm{TM}}$ Generator is composed of a permanent magnet generator (PMG), a compressor, and a turbine mechanically linked to a common shaft and thermodynamically linked to the fuel cell process. The shaft is modeled via Newton's second law for rotation:

$$J\frac{d\omega}{dt} = \sum \tau_i = \tau_T - \tau_C - \tau_G \tag{5a}$$

where J is the turbine's moment of inertia; ω is the angular speed of rotation; and τ_T, τ_C, and τ_G are, respectively, the torques of turbine, compressor, and generator. The torques of turbine and compressor are computed from steady-state energy balances according to:

$$\tau_{T,C} = \frac{P_{T,C}}{\omega} = \frac{\dot{m}_{CT}[\bar{h}(T_{T,C}^{\mathrm{out}}) - \bar{h}(T_{T,C}^{\mathrm{in}})]}{\omega} \tag{5b}$$

where $\dot{m}_{CT}$ is the mass flow through compressor and turbine, obtained from proprietary operating maps. The outlet temperatures of compressor and turbine are obtained from the definitions of the isentropic efficiencies of compression and expansion, which are computed from the operating maps:

$$\eta_C = \frac{(T_{\mathrm{out}}/T_{\mathrm{in}}) - 1}{(p_{\mathrm{out}}/p_{\mathrm{in}})^{1-1/\kappa} - 1}$$

and

$$\eta_T = \frac{(p_{\mathrm{out}}/p_{\mathrm{in}})^{1-1/\kappa} - 1}{(T_{\mathrm{out}}/T_{\mathrm{in}}) - 1}$$

The PMG generates AC power at a variable frequency that is a function of the rotor speed. To convert this into grid AC at 480V/60Hz, the AC power is first rectified to DC power and then inverted to AC power of the desired properties. As the dynamics of the rectification are very fast, they can be neglected. To simplify the model, the permanent magnet generator and rectifier are approximated as a DC motor.[15] DC power is then inverted to grid AC assuming a fixed inverter efficiency. The generator torque is given by:

$$\tau_{\mathrm{G}} = K_m I_G$$

where K_m is the armature constant and I_G is the generator current, which is computed from Ohm's Law as a function of terminal voltage V_t, the induced voltage V_{emf}, and the armature resistance R:

$$I_G = \frac{V_{\mathrm{emf}} - V_t}{R}$$

where the back electromotive force V_{emf} is proportional to the angular rate of rotation:

$$V_{\mathrm{emf}} = K_b \omega$$

Dynamic simulation and conventional control strategy

A dynamic model for the DFC/T system is implemented in Matlab/Simulink using a modular approach (Figure 3). Each unit operation is implemented as a separate Simulink block. As the framework is modular, different system concepts can easily be put together and tested. Since the overall power plant model is a DAE system, initial conditions are required for dynamic simulation purposes. Initial conditions are based on state values during nominal operating conditions. In addition, special attention has been given to making the code robust to inconsistent initial conditions. The simulation includes only principal dynamics, excluding noise or other exogenous disturbances besides electrical loading. In the conventional operating mode, control loops are closed using standard PID elements for the following controlled variables: stack power, fuel flow, water flow, cathode inlet temperature, and micro-turbine speed.

The overall control strategy is implemented by the following control loops:

(1) Stack power is controlled by manipulating the stack current density (i_{stack}). Alternatively, this loop can be opened and the stack current density determined based on the power demand. This would result in i_{stack} being a control variable for dynamic optimization purposes.

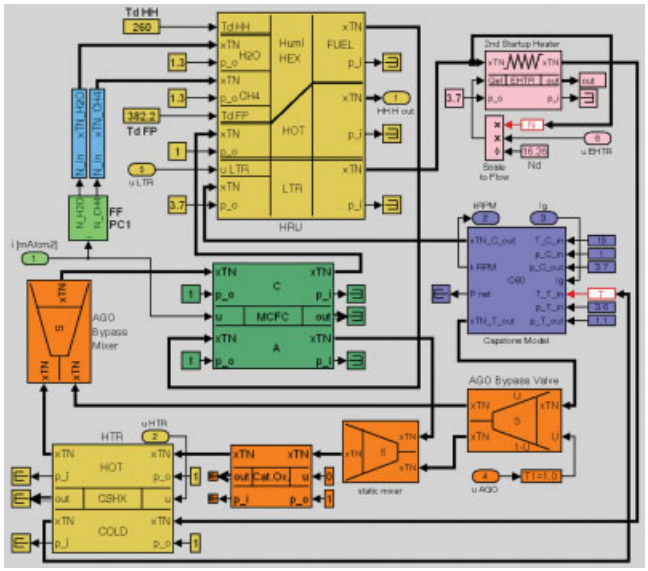

Figure 3. Modular DFC/T Simulink process model.

[Color figure can be viewed in the online issue, which is available at www.interscience.wiley.com.]

(2) Based on off-line generated look-up tables that have been optimized for fuel cell stacks, natural gas fuel flow is controlled to a current-dependent setpoint, which corresponds to target fuel utilization. We will continue to impose this relationship for the dynamic optimization problem. As a result, the problem of determining the optimal feed flow is transformed to a problem of determining an optimal i_{stack} trajectory.

(3) Steam flow is controlled to maintain a target steam/fuel ratio. Steam flow is controlled as a function of methane flow to prevent carbon deposition on the fuel cell's catalyst. This steam-to-carbon ratio is a function (look-up table) of the stack current density. As a result, the steam flow is indirectly controlled by manipulating the stack current density.

(4) Stack cathode inlet temperature is controlled directly by the HTR bypass valve (f_{HTR}) and indirectly by the AGO bypass valve (f_{AGO}; see Figure 1). Depending on the need, auxiliary heat (Q_{EHTR}) can also be provided by an electric heater. The load-dependent cathode inlet temperature setpoint is increased at part-load to compensate for lower cell exothermic heat.

(5) Speed control of the micro-turbine is built into Capstone's control system such that the DFC/T's control system only provides a speed setpoint. In this model, speed control is accomplished by manipulating the generator's terminal voltage (V_T), which is a common control strategy for DC motors.[15]

Dynamic Optimization

Reformulation for dynamic optimization

The process optimization model is based on the existing Simulink model. This DAE model was reformulated to index one using the method of Mattson and Söderlind,[16] discretized with an implicit Runge-Kutta method (Radau collocation),[17] and implemented (modeled) in AMPL.[18] The DAE model of the stack (mass and energy balances Eqs. 1–3) can collectively be represented as follows:

$$M(y,t)\frac{dy}{dt} = f(y,t) \tag{6}$$

where

$$M = \begin{bmatrix} N_c I & & & & \\ & 1 & & & \\ & & N_a I & & \\ & & & 0 & \\ & & & & 0 \end{bmatrix}, \quad y = \begin{bmatrix} x_c \\ T_{\text{stack}} \\ x_a \\ r_1 \\ r_2 \end{bmatrix},$$

$$f = \begin{bmatrix} f_c \\ f_T \\ f_a \\ K_1 x_{a,2} x_{a,5} - x_{a,3}(x_{a,1})^3 p_a^2 \\ K_2 x_{a,3} x_{a,5} - x_{a,4} x_{a,1} \end{bmatrix} \tag{7}$$

where N_a and N_c are the anode and cathode molar hold-ups, respectively; x_a and x_c are the anode and cathode mole fraction vectors, respectively; K_1 and K_2 are the equilibrium constants for the reformation and water gas shift reactions, respectively; T_{stack} is the absolute stack temperature; and p_a is the absolute anode pressure.

The first step in the reformulation is the introduction of new algebraic variables:

$$\bar{y} = \frac{dy}{dt} \tag{8a}$$

This transformation converts the above system to an algebraic equation:

$$M(y,t)\bar{y} = f(y,t) \tag{8b}$$

The two algebraic equilibrium relations in Eq. 7 are differentiated with respect to T:

$$\frac{dK_1}{dT}\bar{T}_{stack}x_{a,2}x_{a,5} + K_1\bar{x}_{a,2}x_{a,5} + K_1 x_{a,2}\bar{x}_{a,5} - [\bar{x}_{a,3}(x_{a,1})^3 + 3x_{a,3}(x_{a,1})^2\bar{x}_{a,1}]\cdot \mathrm{p}_a^2 = 0 \tag{9}$$

$$\frac{dK_2}{dT}\bar{T}_{\text{stack}}x_{a,3}x_{a,5} + K_2\bar{x}_{a,3}x_{a,5} + K_2 x_{a,3}\bar{x}_{a,5} - \bar{x}_{a,4}x_{a,1} - x_{a,4}\bar{x}_{a,1} = 0 \tag{10}$$

and are added to the algebraic system (Eq. 8b). Because two equations were added, two other equations need to be eliminated, such as from the anode mass balance. In this case, the equations for hydrogen and methane, $x_{a,1}$ and $x_{a,2}$, were eliminated from the set of equations (Eq. 8a). To make the DAE system consistent with the constraint:

$$\sum_{i=1}^{7} x_{a,i} = 1 \tag{11a}$$

$x_{a,3}$ is obtained from the above equation. In turn, a third equation (mass balance ODE for $x_{a,3}$) was eliminated. These

quantities can be calculated directly from the algebraic equations. A new set of variables is defined by the following equations:

$$z=\begin{bmatrix} x_c \\ T \\ w \end{bmatrix}, \quad w=\begin{bmatrix} x_{a,4} \\ \vdots \\ x_{a,7} \end{bmatrix} \text{ and } \bar{w}=\begin{bmatrix} \bar{x}_{a,4} \\ \vdots \\ \bar{x}_{a,7} \end{bmatrix}, \quad \bar{z}=\begin{bmatrix} \bar{x}_c \\ \bar{T} \\ \bar{w} \end{bmatrix} \tag{11b}$$

resulting in a set of differential equations:

$$\frac{dz}{dt}=\bar{z} \tag{11c}$$

The initial conditions for the differential variables, *z(0),* can now be set independently; and the algebraic variables, r_1, r_2, $x_{a,1}$, $x_{a,2}$, $x_{a,3}$, and $\overline{y}$ can be solved from Eqs. 8–11.

To improve the calculation efficiency and accuracy in AMPL, the DAE system is scaled using the following techniques:

1. The models consist of different variables of varying scales. To facilitate convergence of the optimization routine to meaningful values, the variables and the constraints were scaled using a single scaling factor θ:

$$T_{\text{scaled}}=\frac{T}{\theta},\ \bar{h}_{\text{scaled}}=\frac{\bar{h}}{\theta},\ c_{\text{p}^{\text{scaled}}}=\frac{c_p}{\theta},\ \dot{x}_{\text{scaled}}=\theta\left(\frac{dx}{dt}\right) \tag{12}$$

2. Because K_1 and K_2 have very small values, a logarithmic transformation is used for efficient numerical calculations. Rather than K_1 and K_2, their logarithms are used directly:

$$\log x_{a,1}=\ln K_2+\log x_{a,3}+\log x_{a,5}-\log x_{a,4} \tag{13a}$$

$$\log x_{a,2}=-\ln K_1+3(\ln K_2)+4(\log x_{a,3})+2(\log x_{a,5}) -3(\log x_{a,4})+2[\log(p)] \tag{13b}$$

Heat exchangers were modeled with ε-NTU formulations (see ref. 14), which require calculation of $\max((mc_p)_a, (mc_p)_b)$ and $\min((mc_p)_a, (mc_p)_b)$ for two exchanging streams *a* and *b*. These non-smooth operators were handled through the smoothing approximations:

$$\max((mc_p)_a,(mc_p)_b)\sim(mc_p)_b +0.2\log_e(1+e^{-5((mc_p)_b-(mc_p)_a)}) \tag{14a}$$

$$\min((mc_p)_a,(mc_p)_b)\sim(mc_p)_a -0.2\log_e(1+e^{-5((mc_p)_b-(mc_p)_a)}) \tag{14b}$$

The remaining dynamic models for oxidizer, micro-turbine, and PID controllers were implemented according to similar guidelines as the stack model. Additional static models, such as mixers, splitters, micro-turbine operating maps, and look-up tables for fuel cell stack operation, are implemented as nonlinear constraints. All models, dynamic and static, follow the same modular approach as the Simulink model, with connections between unit operations modeled via a separate set of equations. This implementation facilitates easy adjustment to changes made to the process flow diagram or conventional control structure.

The overall model of the plant can be described by a system of DAEs. This DAE system also includes algebraic equations that represent the actuator-saturation behavior associated with controllers for output $\alpha(t)$, given by the relations similar to:

$$\alpha(t)=\begin{cases} 0 & \text{if } \beta(\text{t})<0 \\ \beta(t) & \text{if } \beta(\text{t})\in[0,1] \\ 1 & \text{if } \beta(\text{t})>1 \end{cases}$$

where $\beta(t)$ is the input to the actuator. Such actuator-saturation equations are a source of discontinuities. We model these equations by using complementarity constraints[19] derived from the relations:

$$\alpha(t)=z_2(t)+(1-z_1(t)-z_2(t))\beta(t)$$
$$z_1(t)=\arg\min_{0\le z\le 1}\{\beta(t)z\} \quad \forall\ t$$
$$z_2(t)=\arg\min_{0\le z\le 1}\{(1-\beta(t))z\} \quad \forall\ t$$

Such complementarity constraints can easily be handled within the framework of AMPL and IPOPT.[20]

Dynamic optimization framework

Constraints and bounds on the various states, such as stack and oxidizer temperatures, have to be respected while performing optimization studies. Such constraints appear as inequality constraints. The objective function (and some additional constraints) depends on the nature of the optimization problem. Since the plant model is a DAE system, the resulting optimization problem is a dynamic optimization problem, which can be stated as follows:

$$\begin{aligned} \text{Min} \quad & \Phi(z(t_f);y(t_f);t_f;q) \\ \text{s.t} \quad & \text{F}\left(\frac{dz}{dt};z(t);y(t);u(t);t;q\right)=0, \quad z(0)=z_0 \\ & G_s(z(t_s);y(t_s);u(t_s);t_s;q)=0 \\ & z^L\le z(t)\le z^U \\ & y^L\le y(t)\le y^U \\ & u^L\le u(t)\le u^u \\ & q^L\le q\le q^u \end{aligned} \tag{15}$$

where Φ is a scalar objective function at final time t_f, *F* are DAE constraints, G_s are additional point conditions at times t_s, $z(t)$ are differential state profile vectors, $y(t)$ are algebraic state profile vectors, $u(t)$ are control state profile vectors, and q is a time independent parameter vector.

To solve this problem, we apply a full discretization (simultaneous) method.[21] This approach discretizes all variables of the DAE system and generates a large-scale NLP that is then solved using a solver tailored for such applications. With this approach, the DAE system is not solved at each NLP iteration; it is only solved at the optimum. The simultaneous approach has advantages for problems with state variable (or path) constraints and for systems where instabilities occur for a range of inputs. In addition, the simultaneous approach can avoid intermediate solutions that may not exist,

are difficult to obtain, or require excessive computational effort.

In this formulation, the continuous time problem is converted into an NLP by approximating the profiles as a family of polynomials on finite elements. Here we use a collocation form with monomial basis functions for the differential profiles. All of these representations stem from implicit Runge-Kutta formulae[17]; the monomial representation is recommended because of smaller condition numbers and smaller rounding errors. Control and algebraic profiles, on the other hand, are approximated using Lagrange polynomials. These methods offer a number of advantages, including:

- Control variables can be discretized at the same level of accuracy as the differential and algebraic state variables. The Karush-Kuhn-Tucker (KKT) conditions of the discretized problem can be shown to be consistent with the variational conditions of the dynamic optimization problem. Finite elements allow for discontinuities in control profiles.[21]
- Collocation formulations allow problems with unstable modes to be handled in an efficient and well-conditioned manner. The NLP formulation inherits stability properties of boundary value solvers.
- Collocation formulations have been proposed with moving finite elements. This allows the placement of elements for accurate breakpoint locations of control profiles as well as accurate DAE solutions.

Dynamic optimization using collocation methods has been used for a wide variety of process applications, including batch process optimization, batch distillation, crystallization, dynamic data reconciliation and parameter estimation, nonlinear model predictive control, polymer grade transitions and process changeovers, and reactor design and synthesis. Moreover, in a number of comparisons, this simultaneous method has generally superior performance for dynamic optimization over competing methods. Additional survey information on this approach can be found in ref. 21.

Framework for Optimal Operating Policies

Given the process model, a generalized optimization framework for off-line trajectory planning was implemented. The optimization is constrained by the plant dynamics, as well as input and output constraints. The objective function for the optimization formulation (Eq. 15) becomes:

$$\min_{y,u}\Phi = \left\|\Lambda_y(y-y_d)\right\|_2^2 + \left\|\Lambda_u \Delta u\right\|_2^2 \qquad (16)$$

This problem formulation was considered for two types of dynamic optimization problems for optimal process operation. First, in *power tracking*, we determine control moves so that desired load trajectories are tracked. We have determined control moves for both ramp and step profiles over various power regimes. We have performed load tracking studies for over 15 different profiles. Problem formulation and results are presented in the following sections. Second, we *maximize efficiency* while tracking load changes. To facilitate this task, we have included an efficiency measure into the objective function, and we track the same load profiles as in the previous cases. The primary goal here is to study if the efficiency of the plant can be improved, while closely tracking the desired load changes.

For these dynamic optimization problems we present two load profiles:

Case 1:

$$P_d(t) = \begin{cases} 300, & 0 \le t < 450 \text{ s} \\ 300 - \frac{2}{3}(t-450), & 450 \le t < 900 \text{ s} \\ \frac{2}{3}(t-450) - 300, & 900 \le t < 1350 \text{ s} \\ 300, & 1350 \le t \le 1800 \text{ s} \end{cases}$$

Case 2:

$$P_d(t) = \begin{cases} 300, & 0 \le t < 40\,\text{min} \\ 225, & 44 \le t < 76\,\text{min} \\ 300, & 76 \le \text{t} < 108\,\text{min} \\ 225, & 108 \le \text{t} < 124\,\text{min} \\ 300, & 124 \le \text{t} < 140\,\text{min} \\ 225, & 140 \le \text{t} \le 160\,\text{min} \end{cases}$$

Power tracking

The objective is to determine inputs so that desired power trajectories P_d(t) can be tracked optimally. To achieve these desired trajectories, the five conventional PID loops discussed in the second section are removed and their corresponding manipulated variables are determined via dynamic optimization in the following ranges:

For the stack current, a range of $0 \le i_{\text{stack}} \le i^0$, where i^0 is the current density at a nominal power of 250 kW. The HTR bypass is defined through its split fraction: $0 \le f_{\text{HTR}} \le 1$, where $f_{\text{HTR}} = 0$ means that the HTR is completely bypassed and $f_{\text{HTR}} = 1$ means that all flow passes through the HTR. Likewise, the anode gas oxidizer split-fraction f_{AGO} is constrained to be between 0 and 1. The split fraction f_{C60} of the micro-turbine's terminal voltage V_t is defined as $V_t = 390 + 100\, f_{\text{c60}}$. with $0 \le f_{\text{C60}} \le 1$. The electric heater duty Q_{EHTR} is constrained between zero and the heater's maximum power output.

We also need to account for the scheduling of certain stack operating parameters as discussed in the second section. Accordingly, the fuel utilization (U_f), the steam-to-carbon ratio (S/C), and the cathode inlet temperature (TCI) are scheduled as a function of current density i_{stack} based on fuel cell stack manufacturer (FuelCell Energy) proprietary data. We perform a polynomial interpolation on the data and convert each look-up table to a closed form expression. The cathode inlet temperature has to be within ± 5.6 K of the desired value, which is a stringent requirement. The catalytic oxidizer temperature has to be bounded above by 871 K, and the micro-turbine has to operate at a speed that is less than 96k RPM. It is important to realize that all these bounds have to hold at all points in time.

The total power P_{net}(t) produced by the plant not only includes the stack and the micro-turbine contributions but also includes the power of the electric start-up heater (Q_{EHTR} in Figure 1). The purpose of dynamic optimization is to determine these five inputs (f_{HTR}, f_{AGO}, Q_{EHTR}, i_{stack}, and f_{C60}) to track desired power profiles $P_d(t)$. We do this by

minimizing a least-squares objective function of the following form:

$$\Phi = \sum_{i=1}^{40}\sum_{j=1}^{2}(P_{\text{net}}(t_{ij}) - P_d(t_{ij}))^2 + \left[\begin{array}{l} 100\sum_{i=1}^{40}(f_{\text{HTR}}(t_{i1}) - f_{\text{HTR}}(t_{i2}))^2 + 100\sum_{i=1}^{40}(f_{\text{C60}}(t_{i1}) \\ -f_{\text{C60}}(t_{i2}))^2 + 100\sum_{i=1}^{40}(f_{\text{AGO}}(t_{i1}) - f_{\text{AGO}}(t_{i2}))^2 \\ +10^{-2}\sum_{i=1}^{40}(Q_{\text{EHTR}}(t_{i1}) - Q_{\text{EHTR}}(t_{i2}))^2 \\ +100\sum_{i=1}^{40}(i_{\text{stack}}(t_{i1}) - i_{\text{stack}}(t_{i2}))^2 \end{array}\right] + \left[\begin{array}{l} 10^{-2}\sum_{i=1}^{40}\sum_{j=1}^{j=2}(f_{\text{HTR}}(t_{ij}) - 1)^2 + 10^{-2} \\ \times\sum_{i=1}^{40}\sum_{j=1}^{j=2}(f_{\text{C60}}(t_{ij}) - 0.5)^2 + 10^{-2}\sum_{i=1}^{40}\sum_{j=1}^{j=2}(f_{\text{AGO}}(t_{ij}) - 1)^2 \\ +10^{-2}\sum_{i=1}^{40}\sum_{j=1}^{j=2}(i_{\text{stack}}(t_{ij}) - i^0_{\text{stack}})^2 \end{array}\right] \quad (17)$$

The first term in this objective is to track the desired power profile. The second term forces the control variables to be constant within each temporal finite element, that is, there is a cost if the controls are not constant within each mesh. The third set of terms is for regularization purposes. Regularization removes any non-uniqueness that may be associated with trajectory planning problems. A 2-point Radau collocation is used in the formulation of the objective function, and 40 equally spaced finite elements are employed.

The resulting NLP (after discretization) has 51,110 variables and 49,750 constraints for both Cases 1 and 2. The NLP corresponding to Case 1 was solved in 1917 CPU seconds (1.4 GHz Pentium M Laptop, 768 MB RAM), and the NLP corresponding to Case 2 was solved in 125 CPU seconds on the same machine.

The results of the dynamic optimization (for Cases 1 and 2) are shown in Figures 4 and 5. We have also fed the inputs predicted by the optimization procedure back to the Simulink model (which also includes the original PID controllers), and we were able to obtain an excellent match between the results of optimization and simulation. This illustrates the applicability of the proposed dynamic optimization for trajectory planning purposes.

Power tracking with optimized efficiency

The purpose of this study is to show how the dynamic optimization framework can be extended to track power while at the same time maximizing the overall plant effi-

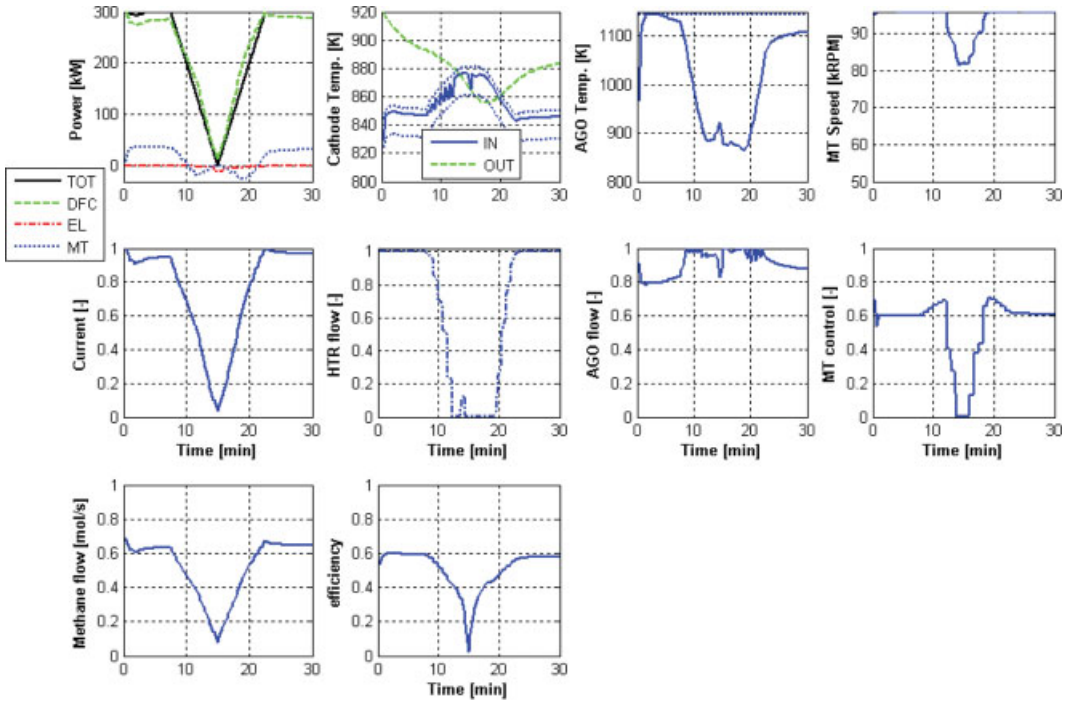

Figure 4. Results for load tracking for Case 1.

Power, temperatures, and micro-turbine speed constitute the first row of plots. In particular, the total power profile (TOT) consists of the direct fuel cell (DFC), the electric heater (EL), and the microturbine (MT). The dotted lines in the second plot are the bounds on TCI. The second row consists of the inputs that have been determined by dynamic optimization, the implementation of which results in the desired load change. The last row consists of the methane flow rate profile and the overall plant efficiency. [Color figure can be viewed in the online issue, which is available at www.interscience.wiley.com.]

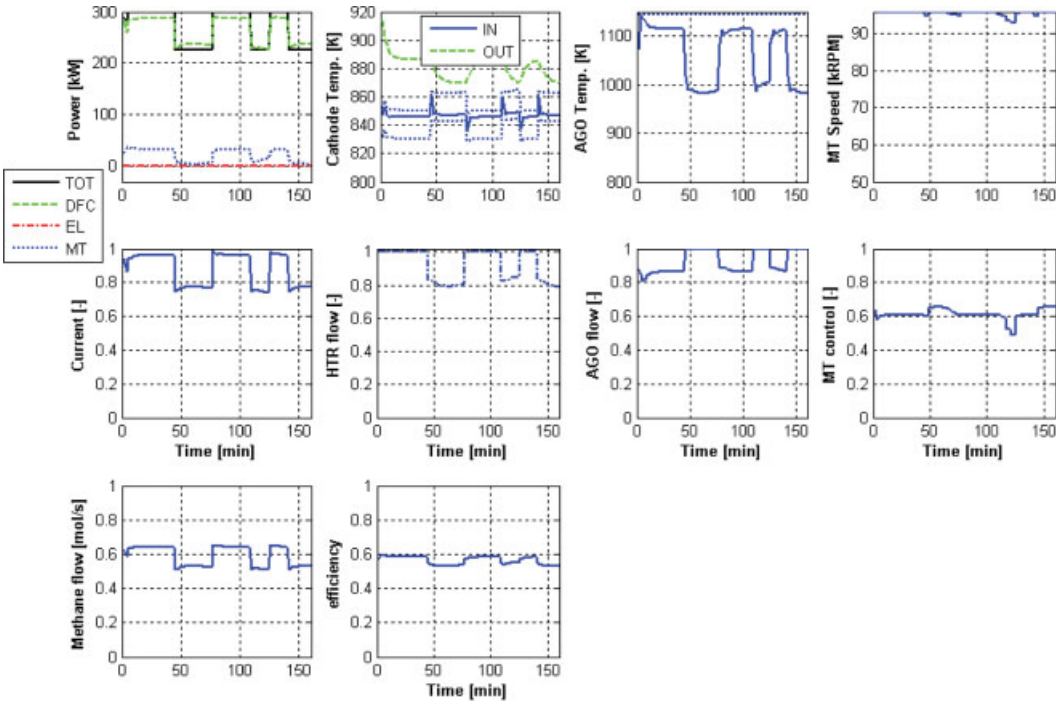

Figure 5. Results for load tracking for Case 2.

Power, temperatures, and micro-turbine speed constitute the first row of plots. In particular, the total power profile (TOT) consists of the direct fuel cell (DFC), the electric heater (EL), and the microturbine (MT). The dotted lines in the second plot are the bounds on TCI. The second row consists of the inputs that have been determined by dynamic optimization, the implementation of which results in the desired load change. The last row consists of the methane flow rate profile and the overall plant efficiency. [Color figure can be viewed in the online issue, which is available at www.interscience.wiley.com.]

ciency. Plant efficiency is defined as:

$$\eta(t) = \frac{P_{\text{net}}(t)}{P_{\text{fuel}}(t)}$$

where P_{net} is the net electric power output and P_{fuel} is the fuel's energy content based on its lower heating value:

$$P_{\text{net}}(t) = \eta_{\text{loss}} * [\eta_{\text{inv}} * P_{\text{dc}}(t) + P_{\text{turbine}}(t)] - Q_{\text{EHTR}}(t)$$

$$P_{\text{fuel}}(t) = \dot{N}_{\text{fuel}}(t) * \text{MW}_{\text{fuel}} * \text{LHV}_{\text{fuel}}$$

where η_{loss} models parasitic losses for blowers and pumps, and η_{inv} is the inverter efficiency. In the second equation, $\dot{N}_{\text{fuel}}(t)$ is the fuel's molar flowrate, MW_{fuel} is the fuel's molecular weight (16 g/mol for methane), and LHV is the fuel's lower heating value (50.0 kJ/g for methane). Clearly we want the efficiency to be as close to one as possible. This implies that $P_{\text{net}}(t)$ should be as close to $800 \cdot \dot{N}_{\text{fuel}}$ as possible, that is:

$$\sum_{i=1}^{40}\sum_{j=1}^{2}\left(P_{\text{net}}(t_{i,j}) - 800 \cdot \dot{N}_{\text{fuel}}(t_{i,j})\right)^2$$

To simultaneously track power, the above term is appended to the objective function for the previous case (Eq. 17) using an appropriate weight ε. In Figure 6 we study the effect of this weight on the solution and determine that a weight of $\varepsilon = 10^{-3}$ is the best trade-off between maximizing efficiency and tracking the desired power profile. Thus, we have incorporated an efficiency measure into the dynamic optimization problem. We have resolved Cases 1 and 2 with this efficiency measure and the results are shown in Figures 7 and 8. The resulting NLP (after discretization) has 51,110 variables and 49,750 constraints for both Cases 1 and 2. The NLP corresponding to Case 1 (with the efficiency term) was solved in 2323 CPU seconds, and the NLP corresponding to Case 2 (with the efficiency term) was solved in 2729 CPU seconds.

Adding this efficiency term can increase the efficiency of the whole plant and, at the same time, track the desired power profile closely. This can be seen, for instance, by comparing Figure 5 with Figure 8. With the added power minimization term, the efficiency increases by 2.7% under full load (from 58.4% to 60%) and by 16% under part load (from 53.5% to 62%).

Optimization Framework for State Estimation

The optimization framework described in the second and third sections can also be used directly to estimate unmeasured inputs and model parameters from measured inputs and outputs using a moving horizon framework. Such moving horizon estimation (MHE) strategies work directly with the nonlinear dynamic model and have been shown to outperform conventional state estimation schemes.[22]

In an analogy to optimization-based control strategies, we again formulate a least squares objective function that is

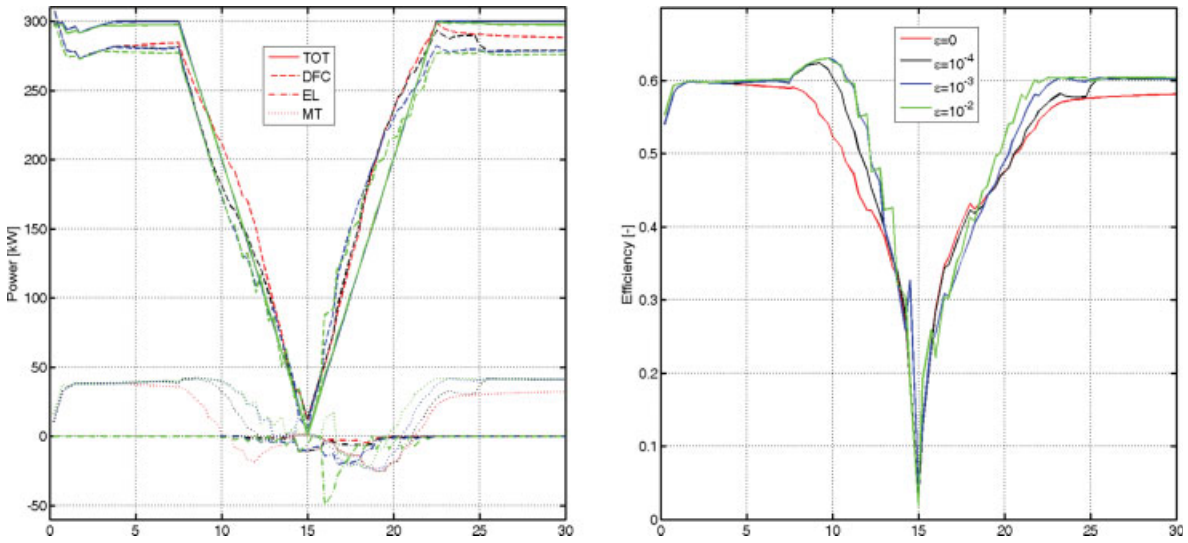

Figure 6. Efficiency and tracked power plots for different weights (for efficiency in the objective function) for Case 1.

The weight 10^{-3} appears to strike the best compromise between an improvement in efficiency and tracking the desired power profile. We have also observed this with several test examples, and as a result will continue to use this weight for future efficiency studies. [Color figure can be viewed in the online issue, which is available at www.interscience.wiley.com.]

applied to the dynamic process model. To evaluate this framework and to explore future directions, we consider composition estimation studies in this section. In the third section, we assumed that pure methane is available as fuel. More often, the fuel does not contain pure methane, but a mixture of methane and other gases. In this study, we consider digester gas, which is a mixture of methane and carbon-dioxide. Typically, the fraction of methane in the digester gas is unknown and subject to change. Research in this direction has focused on dynamic optimization methodologies for estimation of the composition of the digester gas. It is critical to determine the fraction of methane as it has a direct effect on the plant efficiency, the operation of the oxidizer, and the stack durability. For control of the steam-to-carbon ratio, only the methane content has to be considered. We also determine which quantities need to be measured to estimate the composition.

For this optimization formulation, we will assume that the unmeasured quantities are observable and rely on standard

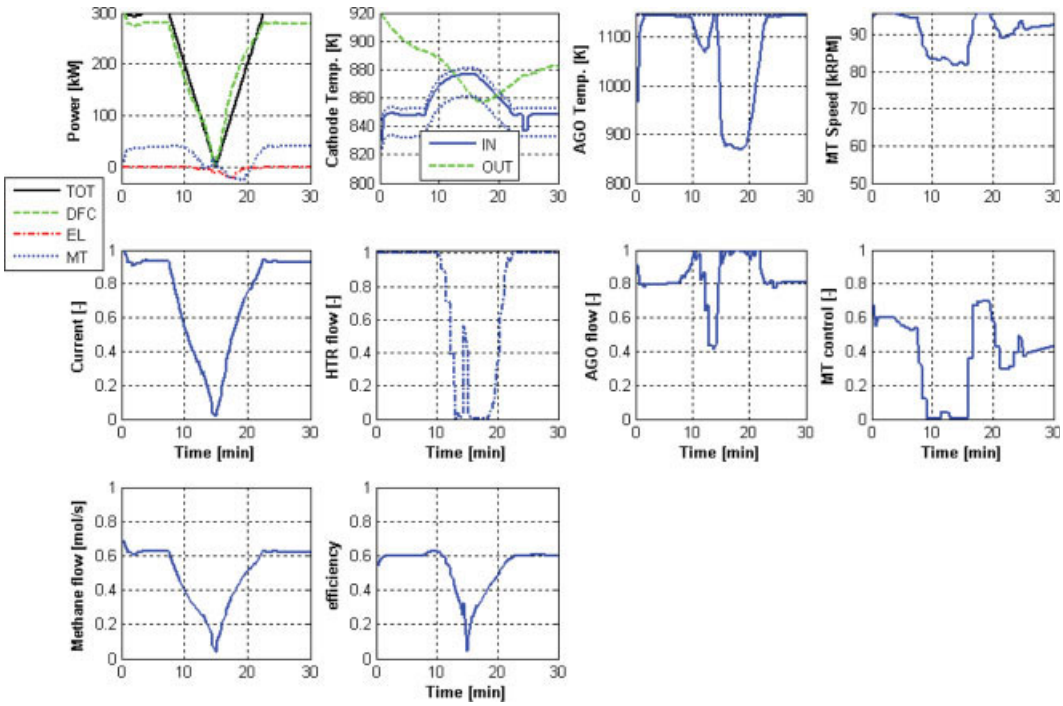

Figure 7. Results for load tracking for Case 1 with the efficiency term included in the objective function ($\varepsilon = 10^{-3}$).

[Color figure can be viewed in the online issue, which is available at www.interscience.wiley.com.]

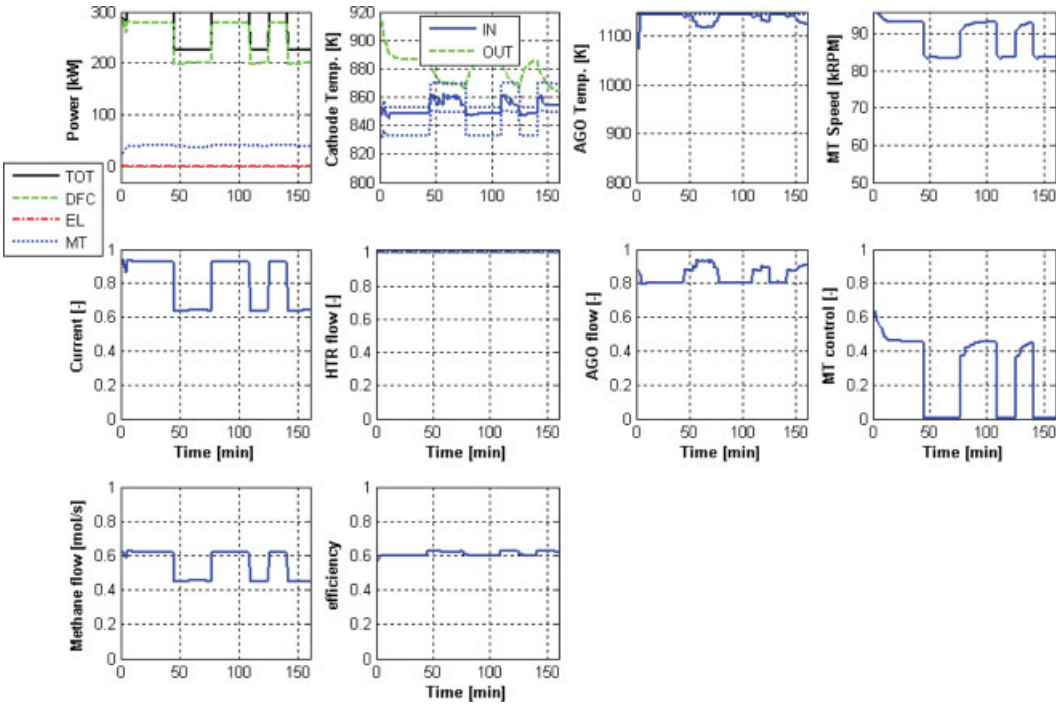

Figure 8. Results for load tracking for Case 2 with the efficiency term included in the objective function ($\varepsilon = 10^{-3}$).

The last row consists of the methane flow rate profile and the overall plant efficiency plot for this case. We can see a clear improvement in efficiency over the results in Figure 5. [Color figure can be viewed in the online issue, which is available at www.interscience.wiley.com.]

observability measures for this analysis.[23] While these measures are developed for linear systems and may be difficult to apply to nonlinear systems, we note that the IPOPT framework allows us to check the observability assumption based on nonsingularity of the KKT matrix at the NLP solution. This allows us to verify whether the unmeasured inputs and parameters are determined uniquely.[20]

Composition estimation studies—MHE problem formulation

The objective of this estimation is to determine methane composition (in digester gas) profiles from available data. A second objective is to determine which quantities should be measured so that the quality of the estimated composition profiles is satisfactory. The inclusion of digester gas as the fuel source, as compared to pure methane in the third section, means that the previously used plant model must be modified.

For this input estimation problem, we consider a time window where digester gas at an unknown composition of methane flows into the system. Let $d_0(t)$ represent the methane composition profile. The estimation problem is posed over this window of time. Either due to prior knowledge or due to information gathered over previous estimation windows, one can assume a predicted concentration profile (typically a constant). Let $\hat{d}(t)$ be the predicted methane composition profile. The methane fraction in digester gas lies typically between 0.5 and 0.7. Based on this, we have set $\hat{d}(t) = 0.6$ in this study. Given the manipulated current density profile $i_{\text{stack}}(t)$, we calculate the theoretical (ideal) methane flow-rate $\dot{N}_{\text{CH}_4}(\text{t})$ that has to go into the plant. If we now divide the theoretical methane flow-rate by the predicted methane composition $\hat{d}(t)$, then we arrive at a predicted digester gas flow-rate. Digester gas at this predicted flow-rate is fed to the plant. But the composition of methane may differ from the predicted concentration; and as a result, the methane flow-rate actually fed to the plant $\dot{N}_{\text{CH}_4}(\text{t})$ is given by:

$$\dot{N}_{\text{CH}_4}(t) = \dot{N}^*_{\text{CH}_4}(t)\,\frac{d_0(t)}{\hat{d}(t)} \tag{18}$$

Depending on how well the actual and the predicted methane compositions match, more or less methane could be fed to the plant. This could adversely affect the performance and the stack durability. As a result, there is a need to estimate $d_0(t)$ (which is equivalent to estimating $\dot{N}_{\text{CH}_4}(t)$). Ideally, this should be done in an on-line manner. In this study, we demonstrate only the proof-of-concept by showing that such an estimation can indeed be performed. While we are not concerned here with computational efficiency, we demonstrate this approach by formulating and solving an off-line dynamic optimization based estimation procedure that estimates the composition profile from available data over an estimation horizon.

Obtaining data

The data used for estimation are obtained from simulations, with known methane composition profiles. We start by including the equation for $\dot{N}_{CH_4}(t)$ (Eq. 18) and other associated modifications in the original dynamic model of the plant. With a given methane composition profile $d_0(t)$, we determine optimal input profiles $i^*_{\text{stack}}(t)$, $f^*_{\text{HTR}}(t)$, $f^*_{\text{AGO}}(t)$, and $f^*_{\text{C60}}(t)$ so that the total power tracks 250 kW over the entire time window (15 min). This can be achieved by using the dynamic optimization framework as in the third and fourth

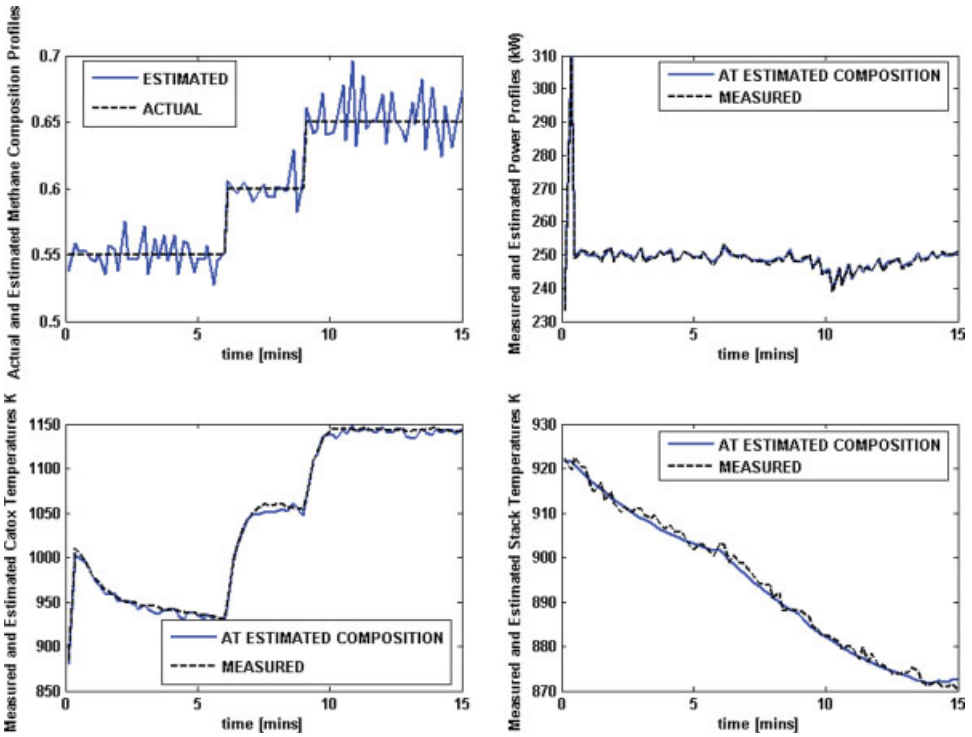

Figure 9. Plots comparing the results of the composition estimation procedure for a step composition profile.

The total power [*kW*] is the only measured variable ($w_{\text{power}} = 10^{-2}$ and $w_{\text{reg}} = 10^{-3}$). We can see that there is a very reasonable agreement between the actual and the estimated methane composition profiles. Also shown (although not used for estimation) are the measured and estimated stack and oxidizer temperatures. [Color figure can be viewed in the online issue, which is available at www.interscience.wiley.com.]

sections. To estimate $d_0(t)$, we choose total power, as well as stack, oxidizer outlet, and anode inlet temperatures as candidates for measured variables. The optimal profiles of these quantities (after adding noise) are then used as measurements. For purposes of testing the estimation procedure, we have obtained data for a time-varying methane composition profile shown in the top-left-hand-corner plot in Figure 9.

Estimation problem

In an on-line setting, the estimation and the control problems are separate, and we try to mimic the same arrangement in our estimation case studies. The estimation window is chosen to be 15 min, and over this horizon we have access to measurement data. The objective of the estimation problem is to determine an estimate ($D_0(t)$) of the true methane composition profile, $d_0(t)$. The estimate should be such that it minimizes the mismatch between model predictions and measured data, and we formulate this as a least-squares objective function:

$$\min_{D_0(t)} \sum_{q\in Q} w_q \sum_{i=1}^{40}\sum_{j=1}^{2}\left(Z_q(t_{ij}) - Z_q^{\text{meas}}(t_{ij})\right)^2 + w_{\text{reg}} \sum_{i=1}^{40}\sum_{j=1}^{2}(D_0(t_{ij}) - 0.6)^2 \tag{19}$$

$$\text{s.t.} \quad \text{Dynamic Model of the Plant} \; (15)$$

Here Z_q are the measured variables, with $q \in Q$; Q is the set of measured variable indices. The first term is the standard least-squares objective function used in estimation problems. We assume we have access to data at all the collocation points, $t_{i,j}$. The second term in the objective is a regularization term for the estimate, to enforce good conditioning of the problem. The weight w_{reg} is typically small ($\sim 10^{-3}$). At this point, it is important to note that since the control and estimation problems are decoupled, the input variables $i_{\text{stack}}(t)$, $f_{\text{HTR}}(t)$, $f_{\text{AGO}}(t)$, and $f_{\text{C60}}(t)$ that were used in the optimization of the dynamic model are set equal to $i^*_{\text{stack}}(t)$, $f^*_{\text{HTR}}(t)$, $f^*_{\text{AGO}}(t)$, and $f^*_{\text{cap}}(t)$, respectively. So the only unknown in the dynamic plant model is $D_0(t)$, and it is chosen so that the least-squares objective function is minimized. The resulting NLP (after discretization) has 47,670 variables and 46,550 constraints.

Case studies

For the prescribed methane profile data, we choose five possible candidates for the set of measured variables. Figure 9 corresponds to the case where the measured variable is total power, that is, $Q = \{P_{\text{net}}\}$. This shows that choosing the total power as the only measured variable is sufficient for the estimation procedure to function reasonably well.

Nevertheless, from structural considerations of the DAE system, we note there are a number of consequences of measurement-parameter relations. For instance, if power is the only output, then the estimated methane composition tracks not only this measurement but also the noise associated with this measurement. Thus, the noise level seems high and there is some mismatch in the stack temperature profiles (Figure 9). The reason for the noisy estimated methane profile is due to

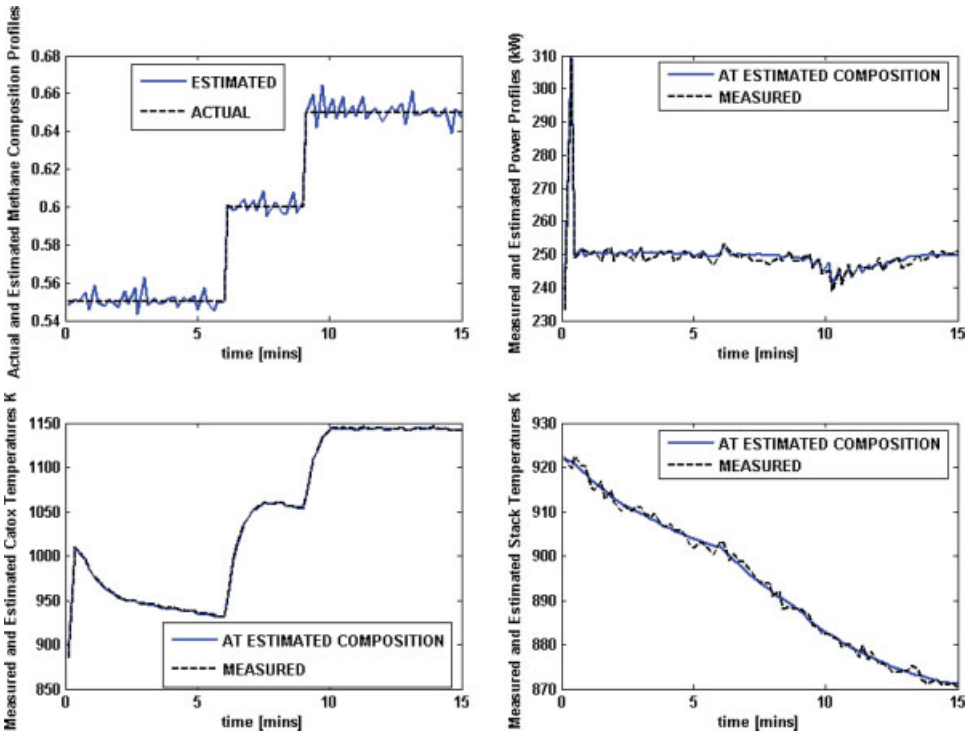

Figure 10. Plots comparing the results of the composition estimation procedure when using three additional measurements.

The total power [*kW*], as well as the stack, oxidizer outlet, and anode inlet temperatures [*K*] are the measured variables ($w_T = 10^{-2}$, $w_P = 10^{-2}$, and $w_{\text{reg}} = 10^{-3}$). We can see that there is a very good agreement between the actual and the estimated methane composition profiles. The other quantities (in particular, the stack temperature) also agree well with the measured data. [Color figure can be viewed in the online issue, which is available at www.interscience.wiley.com.]

a highly algebraic structural relationship in Eq. 4. For instance, when power is measured and current density is known, then the cell voltage is calculated immediately. Moreover, because the relationship between the cell voltage and composition of the various components is given by a set of mostly-algebraic equations (that is, without dynamics), then the cell voltage and, as a result, the composition of the components going into the stack, can track the noise levels in the measured power directly. Adding more measurements mitigates the effect of this algebraic structure, by adding dynamic lags that smooth the noise. To demonstrate this, Figure 10 shows that the addition of the stack, oxidizer outlet, and anode inlet temperatures reduces the noise level in the estimated profile and produces a good match between the measured and the calculated variable profiles. Choosing measured variables for parameter estimation is also governed by a number of other considerations. A more thorough investigation is discussed in the next section and left for future work.

Conclusions

An optimization based framework to determine optimal operating policies for hybrid fuel cell/gas turbine power systems has been developed. The approach considers a dynamic model of the system, reformulated as an index 1 DAE. The system model is discretized using Radau collocation (a high order implicit Runge-Kutta method) and formulated in the AMPL modeling environment. This allows for the straightforward solution of a dynamic optimization problem using large-scale nonlinear programming (NLP) solvers; the IPOPT solver was used for this project. Program links were provided to Matlab/Simulink to visualize and interpret the results.

The approach was demonstrated for the optimization of operating conditions, especially in tracking load changes and also with efficiency measures included as part of the optimization model. Results from 18 cases showed that the dynamic optimization could be performed quickly with excellent results. The optimization framework was also demonstrated for the estimation of feed fuel concentrations. This provides a demonstration of the dynamic optimization formulation for state and parameter estimation problems for this fuel cell based process.

The results described in this work demonstrate that the optimization framework can be used for a wide variety of applications, including:

- Optimal policies for different operating scenarios
- Maximizing efficiencies for transient and steady state operation
- Optimal rejection of disturbances
- Estimation of unmeasured disturbances, process faults, and drifting model parameters

A number of issues also need to be explored for future work. In particular, several improvements can be made in the optimization framework. Because the process model leads to

a highly nonlinear formulation, improvements can be made in modeling non-smooth terms and poorly behaved functions (such as square roots, logarithms) and complementarity conditions. In this work, considerable care was taken in formulating these terms. However, with further experience, additional improvements can also be implemented, including a systematic and automatic initialization of the NLP problem. In addition, the on-line implementation of this optimization strategy will be realized within a moving horizon framework as a flexible general-purpose nonlinear model predictive controller. With the addition of more efficient initialization strategies for the dynamic optimization, computational times can be further reduced. Moreover, this approach can directly leverage recent computational advances in this area, both for nonlinear MPC[24] and moving horizon estimation.[25] Also, the model in this study has well-characterized parameters with little uncertainty. Nevertheless, as the model is refined and additional parameters and uncertain inputs are added, off-line dynamic optimization can be extended to consider sensitivity studies as well as robust optimization formulations, as described in ref. 26.

Similar improvements can be realized in the related task of on-line identification. As mentioned above, we assume that the set of outputs is chosen so that the desired parameters are observable. However, the appropriate choice of outputs for parameter estimation depends on a number of factors:

- Referring to Eq. 19, an obvious metric in choosing outputs is to maximize the information, as defined by log(det(V)), where V is the covariance of the estimated parameters. If the measurements have independent errors, we can represent this covariance to a first approximation by:

$$V(p) = \sum_{q \in Q} (\sigma_q)^2 \sum_{ij} \left[\left(\frac{\partial Z_q(t_{ij})}{\partial p} \right) \left(\frac{\partial Z_q(t_{ij})}{\partial p} \right)^T \right]^{-1} \tag{20}$$

Two observations follow immediately. First, the information content increases with the number of measurements. Second, the dominant terms in the outer summation correspond to those measurements with the most influence on the information content. Therefore, the choice of the best measurement can be based on the dominant term in the outer summation in Eq. 20.

- Another approach to assessing an appropriate choice of measurements would be through the construction of a Luenberger observer or extended Kalman filter.[23] While this approach is limited to only linearized models, and can only lead to approximate parameter estimates, it can still serve as a metric to choose good measurements. Here one could rewrite the linearized dynamic model with parameters as additional states, described by the equations: $\dot{p} = 0$. Coupled with the controller, outputs can be chosen so that the best estimator can be designed to converge quickly to a desirable set of parameters. For linear models, this can be done independently of the controller design.

In summary, the application of an efficient simultaneous dynamic optimization approach has led to an efficient and effective strategy to determine optimal operation strategies. Our planned future work will directly lead to superior on-line estimation and control strategies as well.

Acknowledgments

Funding from the U.S. Department of Energy through NETL under contract DE-FG02-02ER86140 is gratefully acknowledged.

Literature Cited

1. Williams MC, Strakey JP, Singhal SC. US distributed generation fuel cell program. *J Power Sources*. 2004;131:79–85.
2. Ghezel-Ayagh H, Walzak J, Patel D, Daly J, Maru H, Sanderson R, Livingood W. State of direct fuel cell/turbine systems development. *J Power Sources*. 2005;152:219–225.
3. Farooque M, Ghezel-Ayagh H. "Part 7: Molten carbonate fuel cells and systems, system design. "*Handbook of Fuel Cells, Fundamentals, Technology and Applications, Volume 4: Fuel Cell Technology and Applications, Part 2*. Vielstich W, Lamm A, Gasteiger H, eds. New York: John Wiley & Sons; 2003:942–968.
4. Lukas MD, Lee KY, Ghezel-Ayagh H. Modeling and cycling control of carbonate fuel cell power plants. *Control Eng Practice*. 2002; 10(2):197–206.
5. Roberts RA, Jabbari F, Brouwer J, Gemmen RS, Liese EA. Interlaboratory dynamic modeling of a carbonate fuel cell for hybrid application. Proc ASME Turbo Expo, Atlanta, GA, 2003, Paper No. GT2003–38774.
6. Lukas MD, Lee KY, Ghezel-Ayagh H. Modeling, simulation, and control of direct reforming molten carbonate fuel cell power plant. The Fourth IFAC Symposium on Power Plants & Power Systems Control, Brussels, Belgium, April 26–29, 2000, pp. 127–134.
7. Litzinger KP, Shockling LA, Veyo SE, Lundberg WL. Comparative evaluation of SOFC/Gas Turbine hybrid system options. Proceedings of ASME Turbo Expo, Reno, NV, 2005, Paper No. GT2005–69119.
8. Tucker D, Lawson L, Smith TP, Haynes C. Evaluation of cathodic air flow transients in a hybrid system using hardware simulation. 4th Int Conf Fuel Cell Science, Engineering and Technology, Irvine, CA, June 19–21, 2006.
9. Ghezel-Ayagh H, Walzak J, Junker ST, Michelson F. Development of SubMW Hybrid Direct FuelCell/Turbine power plant. 2005 Fuel Cell Seminar, Palm Springs, CA, Nov. 14–18, 2005.
10. Ghezel-Ayagh H, Daly JM. Progress in development of direct FuelCell/Turbine® systems. Proc 27th Int Tech Conf Coal Utilization & Fuel Systems, Clearwater, FL, March 4–7, 2002.
11. Ghezel-Ayagh H, Daly JM, Wang Z. Advances in direct FuelCell®/Gas Turbine power plants. Proc ASME Turbo Expo, Atlanta, GA, June 16–19, 2003, Paper No. GT2003–38941.
12. Ma Z, Blanchet S, Venkataraman R, Iaccarino G, Moin P. Mathematical modeling of an internal-reforming carbonate fuel cell stack. 2nd ASME Int Conf Fuel Cell Science, Engineering and Technology, Rochester, NY, June 2004.
13. Lukas MD, Lee KY, Ghezel-Ayagh H, Abens SG, Cervi MC. Experimental transient validation of a direct FuelCell® stack model. Proc 2001 IEEE Power Engineering Society Summer Meeting, Vancouver, 2001.
14. Incropera FP, DeWitt DP. *Fundamentals of Heat and Mass Transfer,* 4th Ed. New York: John Wiley & Sons; 1981.
15. Mohan N, Undeland TM, Robbins WP. *Power Electronics. Converters, Applications, and Design,* 2nd Ed. New York: John Wiley & Sons; 1995.
16. Mattsson SE, Söderlind G. Index reduction in differential-algebraic equations using dummy derivatives. *SIAM J Sci Comp*. 1993;14: 677–692.
17. Ascher UM, Petzold LR. *Computer Methods for Ordinary Differential Equations and Differential-Algebraic Equations.* Philadelphia, PA: SIAM; 1998.
18. Fourer R, Gay D, Kernighan B. *AMPL*. South San Francisco: The Scientific Press; 1993.
19. Raghunathan AU, Biegler LT. Mathematical Programs with Equilibrium Constraints (MPECs) in process engineering. *Comput Chem Eng*. 2003;27(10):1381–1392.
20. Wächter A, Biegler LT. On the implementation of a primal-dual interior point filter line search algorithm for large-scale nonlinear programming. *Math Prog*. 2006;106:25–57.

21. Kameswaran S, Biegler LT. Simultaneous dynamic optimization strategies: recent advances and challenges. *Computers Chem Eng*, 2006;30:1506–1575.
22. Rawlings JB, Bakshi BR. Particle filtering and moving horizon estimation. *Comp Chem Eng*. 2006;30:1529–1541.
23. Kwakernaak H, Sivan R. *Linear Optimal Control Systems*. New York: Wiley-Intersci.; 1972.
24. Zavala VM, Laird CD, Biegler LT. Fast solvers and rigorous models: can both be accommodated in NMPC? 2006 *J Robust and Nonlinear Control*, submitted for publication.
25. Zavala VM, Laird CD, Biegler LT. A fast computational framework for large-scale moving horizon estimation, 2006 *Dy COPs* 07, submitted for publication.
26. Laird CD, Biegler LT. Large-scale nonlinear programming for multi-scenario optimization, 2006 High performance Supercomputing, Lecture Notes on Computational Science and Engineering, Springer, Berlin, accepted for publication.

Manuscript received July 18, 2006, and revision received Dec. 3, 2006.